On Thin or Slender Bodies

by E.O. Tuck
The University of Adelaide, South Australia 5005

(to be presented as Lighthill Lecture,
BAMC, Norwich, April 2004)

DRAFT

February 18, 2004

Abstract

A review of thin-body and slender-body theories, with indications of some new applications. Topics discussed include bodies with near-constant surface pressure, subsonic and supersonic aerodynamics, ship hydrodynamics, slender bodies in Stokes flow, slender footings in elastic media, and slender moonpools. Mathematical features of the thin and slender body approximations are also discussed, especially non-local convolution terms modelling three-dimensionality in the otherwise two-dimensional near field, end effects, and the role of the logarithm of the slenderness ratio.

Introduction

This paper mainly concerns fluids streaming past about impermeable elongated bodies, a topic which has always been one of the most important in fluid mechanics, and one to which Sir James Lighthill contributed substantially, from his earliest research days in the 1940s. However, there are also potential or actual applications in other areas including solid mechanics.

Within fluid mechanics, most of this paper concerns irrotational potential flow of an inviscid incompressible fluid, but again there are many other fluid-mechanical applications, e.g. to subsonic and supersonic compressible flows, and to very viscous Stokes flows. The potential flow demands solution of an exterior boundary-value problem for Laplace's equation, with a Neumann boundary condition on the fixed body surface.

Even when there is just one such boundary surface, solution of this type of boundary-value problem for geometrically complex bodies presented major computational difficulties until relatively late in the 20th century, and hence there was often a resort to approximations based on simplifying geometrical features to the body. Fortunately, in many real applications there are indeed such features present, namely the body is elongated in the flow direction, or "streamlined". [Incidentally, that now-common English word "streamlined" has a technical origin involving the body geometry conforming to flow streamlines, and this tells us that there is no element of luck about the presence of geometrical simplifying features!] Streamlined bodies are usually either thin (approximated by a plane) or slender (approximated by a line).

Nowadays, the tools of computational fluid dynamics are such that this type of boundary-value problem is almost trivially solvable, and one might question the need to use such approximations. However, there are often other reasons for their retention. One such reason is that there may be other boundaries – other bodies, or more importantly other boundaries such as free surfaces. The problem of flow past a ship or submarine is one such example, and the nonlinear boundary conditions on a free-surface that is not known in advance present serious difficulties to any computational procedure, even with 21st century computers.

Just to set that scene, Figure 1 shows some ship waves computed in a few minutes of 2GHz PC time using a thin-ship approximation (Tuck, Scullen and Lazauskas 2002). These computations are for a vessel which approximates in size, shape and speed the ship in the photograph of Figure 2. Capturing the full complexity of a ship-wave pattern is a challenge even after the thin-ship approximation has been made – without that approximation, compromises have to be made that may be unacceptable in some applications, e.g. to detection.

We shall return to problems involving free surfaces and other generalisations later, but first let us discuss the most straightforward flow situation, which requires solution of a Neumann problem for Laplace's equation exterior

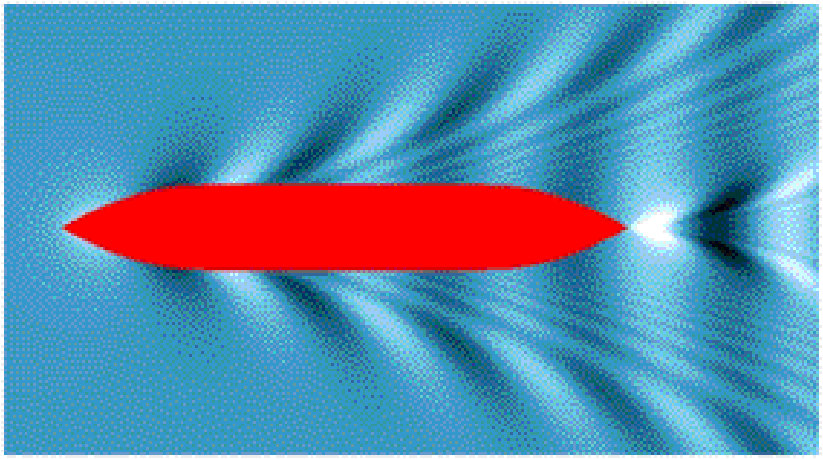

Figure 1: Computed ship waves.

to a single body. For definiteness we shall call this the "prototype" problem.

Interior sources

Among the many ways to solve Neumann boundary-value problems, one of the oldest is to place singularities inside the body, whose strength is to be determined. We shall only be concerned with non-lifting bodies here, so these singularities can be assumed to be sources. This concept generalises the Rankine body, which is generated by one source and one equal sink. Good numerical methods can then be devised both in two and three dimensions for arbitrary bodies, with a careful placement of many sources. The source distribution may be discrete or continuous; let us here assume the latter. In the most general case, it is best that the sources lie not too far inside the

Figure 2: Actual ship wave photograph.

body, and in particular, if they lie on the (inside of the) body itself, such methods reduce to "boundary integral equation" or "panel" methods.

However, there is a significant class of smooth and not-too-fat bodies for which this principle of closeness to the body surface can be violated without cost. For most laterally symmetric bodies the sources can be placed on the plane of symmetry, and for most bodies of revolution they can be placed on the axis.

Thus for a body alone in two dimensions we may suggest

$$\phi(x,y) = \frac{1}{2\pi} \int m(\xi) \log \sqrt{(x-\xi)^2 + y^2}\, d\xi \tag{1}$$

and for a body of revolution (with r as a polar coordinate normal to the axis)

$$\phi(x,r) = -\frac{1}{4\pi}\int \frac{m(\xi)}{\sqrt{(x-\xi)^2+r^2}}\,d\xi \tag{2}$$

The integrals in each case take place over a suitable range of ξ values inside the body. For finite bodies, we shall often take this range to be $(-1,1)$, but in principle $(-\infty,\infty)$ can be assumed, with truncation to a finite range if $m(\xi)$ vanishes outside that range. Here ϕ is the potential for the disturbance to a unit-magnitude x-directed stream due to the body, such that the total fluid velocity is $\mathbf{q} = \nabla(x+\phi)$. The only remaining requirement is that the Neumann boundary condition $\mathbf{q}.\mathbf{n} = 0$ is satisfied on the body surface, leading to an integral equation for the source strength function $m(\xi)$.

For example, in the 3D case on $(-1,1)$, the linearly-varying function

$$m(\xi) = -2\pi\epsilon^2\,\xi \tag{3}$$

generates the exact solution for flow over a spheroid which extends somewhat beyond the sources, to $|x| = \zeta$ with $\zeta > 1$, and has a maximum radius $r = \sqrt{\zeta^2-1}$, where $\epsilon^2 = -\left[Q_1'(\zeta)\right]^{-1}$, with

$$Q_1(\zeta) = \frac{1}{2}\zeta\log\frac{\zeta+1}{\zeta-1} - 1 \tag{4}$$

a Legendre function of the second kind. We shall explore this exact solution further later. For small ϵ, we have $\zeta \approx 1+\epsilon^2/2$, and the spheroid is slender, with maximum radius/half-length approximately equal to ϵ.

One primitive but often quite successful version of slender-body theory simply says the following. When the body is expanding its cross-section area, each unit-length section occupies an extra volume equal to the rate of increase in section area, and that is volume lost to the stream. To conserve mass, there must therefore be an outward flux or source strength equal to the stream magnitude U times that volume. Hence $m(\xi)$ is approximately equal to U times the x-wise rate of change of body section area at station $x = \xi$. Thus for a body of revolution $r = f(x)$ with section area πf^2 in a unit stream $U = 1$, we have

$$m(\xi) = 2\pi f(\xi) f'(\xi) \tag{5}$$

In 2D, section area is replaced by body thickness, so for a symmetric 2D body $y = \pm f(x)$ with thickness $2f$ in a unit stream we have

$$m(\xi) = 2f'(\xi) \tag{6}$$

Once $m(\xi)$ is so specified, in principle there is no need for further approximation, and the flow is fully determined. However, let us explore systematic theories in which not only are the source strengths correctly determined by the above formula to a leading-order approximation, but further consistent approximations are made in determining flow quantities of interest such as the pressure distribution on the body.

Thin symmetric bodies in 2D

A consistent thin-body theory for the symmetric body $y = \pm f(x)$ demands that we consider the limit as $f(x) \to 0$, in which the body shrinks to the plane $y = 0$. The limiting form of the Neumann boundary condition is then

$$\phi_y(x, 0_\pm) = f'(x) \tag{7}$$

on the top and bottom sides of the limiting plane boundary $y = 0$. This boundary condition is satisfied exactly by the expression (1), providing $m(\xi)$ is given by (6).

The main output is then the pressure distribution (excess over atmospheric) on the body, which is given (neglecting second-order terms) by Bernoulli's equation as

$$p(x) = -\phi_x(x, 0_\pm) \tag{8}$$

Both the fluid density and the stream velocity have been normalised to unity; the non-dimensional quantity $p(x)$ used here is then half of the usual pressure coefficient. Note that not only have we neglected the square of the lateral velocity ϕ_y, but also we have consistently evaluated the pressure on the limiting plane boundary $y = 0_\pm$ rather than the actual boundary $y = \pm f$. Then using (1) and (6) we find that the pressure is the Hilbert transform of the body slope, namely

$$p(x) = -\frac{1}{\pi} \int \frac{f'(\xi)}{x - \xi} d\xi \tag{9}$$

This is a "small" pressure disturbance, of the same (first-order) magnitude as the body thickness f. The relationship (9) between shape f and pressure

p is linear, and if $f = O(\epsilon)$ for some small parameter ϵ, then also $p = O(\epsilon)$, with error $O(\epsilon^2)$.

For example, on $(-1, 1)$ the elliptic cylinder

$$f(x) = \epsilon\sqrt{1 - x^2} \tag{10}$$

gives according to (9) the constant negative pressure $p = -\epsilon$. This is clearly not a good approximation near the ends of the body (where we should find stagnation pressure $p = +1/2$), a matter to which we shall return later.

There are many properties of Hilbert transforms that can be used to generate interesting results for pressures on thin bodies. For example, since an analytic inverse Hilbert transform is known, we can immediately write down the body slope generating a given pressure distribution. On the full infinite range, we have

$$f'(x) = \frac{1}{\pi}\int_{-\infty}^{\infty} \frac{p(\xi)}{x - \xi} d\xi \tag{11}$$

and on the finite interval $(-1, 1)$, we have

$$f'(x) = \frac{1}{\pi\sqrt{1 - x^2}}\int_{-1}^{1} \frac{\sqrt{1 - \xi^2}\, p(\xi)}{x - \xi} d\xi \tag{12}$$

(assuming $f = 0$ for all $|x| \geq 1$).

Slender bodies of revolution

Not everything follows as easily for slender bodies as it does for thin bodies! Essentially this is because the limiting line is a one-dimensional object, and therefore cannot serve as a boundary for the limiting 3D boundary-value problem. Instead of letting the body shrink fully down to the limiting line $r = 0$, we must instead match with an "inner" flow for small but nonzero r.

We therefore need the behaviour of the potential (2) for small r, namely

$$\phi(x, r) = \frac{m(x)}{2\pi} \log r + b(x) + O(mr^2 \log r) \tag{13}$$

where

$$b(x) = -\frac{1}{4\pi}\int m'(\xi)\, \mathrm{sgn}(x - \xi) \log 2|x - \xi|\, d\xi \tag{14}$$

The logarithmic part of (13) is easy to understand – a line of 3D sources behaves near that line as if it was a 2D line source with the local source strength. However, if the source strength $m(x)$ varies with x, then there will be non-zero and non-trivial axial (x-wise) fluid motion which is determined by the non-local term $b(x)$. Equation (14) applies both to finite and infinitely-long bodies. If the body is of finite length, e.g. occupies $|x| < 1$, a careful integration by parts yields the alternative formula

$$b(x) = -\frac{m(x)}{2\pi} \log 2\sqrt{1-x^2} + \frac{1}{4\pi} \int_{-1}^{1} \frac{m(x) - m(\xi)}{|x-\xi|}\, d\xi \tag{15}$$

Again, immediate substitution of (13) in the approximate Neumann boundary condition $\phi_r = f'(x)$ on $r = f(x)$ verifies the slender-body approximation (5) for the source strength $m(x)$.

Note that $m = O(\epsilon^2)$ if $f = O(\epsilon)$, i.e. if ϵ measures slenderness, and hence the full disturbance potential given by (2) is also of second order, with $\phi = O(\epsilon^2)$. The inner approximation (13) to ϕ with $r = O(\epsilon)$ is strictly then of order $\epsilon^2 \log \epsilon$. This type of extra "$\log \epsilon$" factor is common in slender body theory, and for some order of magnitude estimation purposes can be ignored, and we then view the disturbance due to the body as simply "second order", even near the body. Similarly, it can be shown that the error in the slender-body approximation (5) to the source distribution is of order $\epsilon^4 \log \epsilon$ or (loosely) "fourth order", and the error in the formula (13) for the disturbance potential near the body is then of order $\epsilon^4 \log^2 \epsilon$, again loosely fourth order. We shall return to matters involving these logarithms later.

Now the Bernoulli equation determines the pressure as

$$p = -\phi_x - \frac{1}{2}\phi_r^2 \tag{16}$$

where we have neglected the (fourth-order) term ϕ_x^2, but now (in contrast to the 2D case) cannot neglect the (second-order) term ϕ_r^2. The whole pressure is then of second order. Substituting the inner approximation (13) gives on the body $r = f(x)$

$$p(x) = -[f(x)f'(x)]' \log f(x) - b'(x) - \frac{1}{2} f'(x)^2 \tag{17}$$

For finite-length bodies on $(-1, 1)$ it is convenient to use (15), with the definitions $A(x) = f(x)f'(x)$ and

$$B(x) = \frac{1}{2} \int_{-1}^{1} \frac{A(x) - A(\xi)}{|x-\xi|}\, d\xi \tag{18}$$

to write the pressure as

$$p(x) = -A'(x)\log\frac{f(x)}{2\sqrt{1-x^2}} - B'(x) - \frac{xA(x)}{1-x^2} - \frac{1}{2}f'(x)^2 \qquad (19)$$

This expression is in some ways equivalent to the Hilbert transform (9) for the corresponding thin-body pressure, and indeed the (linear) integral transform (18) connecting $A(x)$ and $B(x)$ plays a similar non-local role. However, now there are significant local terms as well, and the full relationship (19) between body geometry and pressure distribution is not linear.

The approximation (19) clearly breaks down at the ends $x = \pm 1$, where it predicts a (positive) infinite pressure. For most finite bodies, the ends will be stagnation points where we expect $p = 1/2$. It should of course be noted that this is not as dramatic a failure as appears at first sight. After all, what (19) is saying is that the pressure on a slender body is small, of second order in ϵ. On such a scale, the finite stagnation pressure appears effectively infinite.

However, both in 2D and 3D it is also possible to construct uniformly valid approximations, and Lighthill (1949) was one of the first to do this in 2D. For slender bodies of revolution $r = f(x)$, this simply involves dividing the pressure given by (19) by

$$1 + \left(\frac{xf(x)}{1-x^2}\right)^2 \qquad (20)$$

which is such as to guarantee stagnation pressure $p = 1/2$ at $x = \pm 1$, but makes a negligible $O(\epsilon^4 \log \epsilon)$ change if $|x|$ is not near 1.

Exact pressure on ellipses and spheroids

If either the elliptic cylinder

$$y = \pm\epsilon\sqrt{1-x^2} \qquad (21)$$

or the spheroid

$$r = \epsilon\sqrt{1-x^2} \qquad (22)$$

is placed in a unit-magnitude stream, the velocity magnitude on its surface is given (exactly) by

$$q = \frac{1+\lambda}{\sqrt{1+\epsilon^2 x^2/(1-x^2)}} \qquad (23)$$

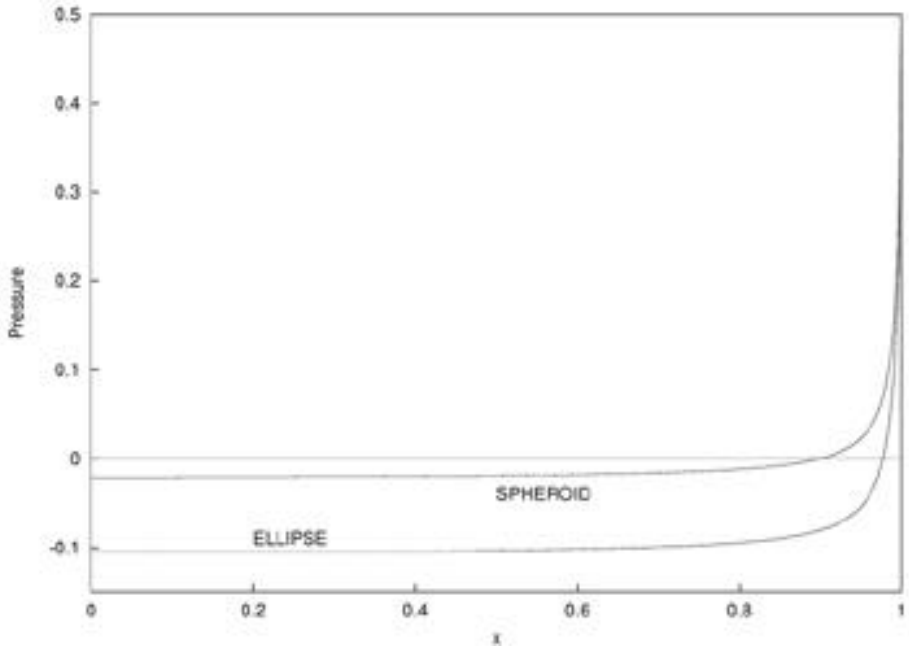

Figure 3: Exact non-dimensional pressure on ellipse and spheroid, each with thickness/length $\epsilon = 0.1$.

where $1 + \lambda$ is the (maximum) velocity, namely that at $x = 0$. This result follows from the exact solutions (Lamb 1932), or simply by careful tangential differentiation of the velocity potential ϕ, which is (exactly) equal to $(1+\lambda)x$ on these bodies (Tulin 1998). The corresponding (non-dimensional) pressure disturbance p is (exactly)

$$\begin{aligned} p(x) &= \frac{1}{2} - \frac{1}{2}q^2 \\ &= \frac{-\lambda - \frac{1}{2}\lambda^2 + \frac{1}{2}\epsilon^2 x^2/(1-x^2)}{1 + \epsilon^2 x^2/(1-x^2)} \end{aligned} \tag{24}$$

Although the same formula (24) yields the surface pressure on ellipses in 2D and spheroids in 3D, the maximum velocity $1 + \lambda$ takes different values in each case. For ellipses of width/length ratio ϵ in 2D flow we have simply

$$\lambda = \epsilon \; . \tag{25}$$

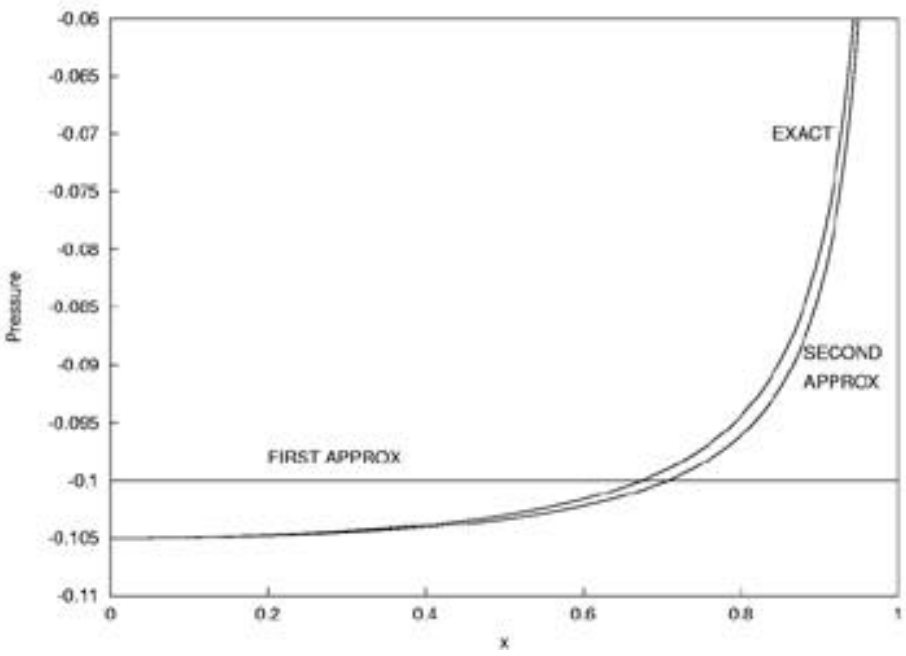

Figure 4: Pressure on ellipse with thickness/length $\epsilon = 0.1$.

The exact result in 3D for spheroids of diameter/length ratio ϵ is a little more complicated, namely

$$\lambda = -\frac{Q_1(\zeta)}{\zeta Q_1'(\zeta)} \tag{26}$$

where $\zeta = (1-\epsilon^2)^{-1/2}$ and $Q_1(\zeta)$ is the Legendre function defined in (4).

Figure 3 shows example computations of $p(x)$ in $x \geq 0$, for $\epsilon = 0.1$. Although these exact pressures eventually return to the (maximum positive) stagnation value $p = 1/2$ at the extreme end $x = 1$, they take small negative values over more than 90% of the length.

Thin ellipses and slender spheroids

We are mainly concerned with thin 2D or slender 3D bodies, for which we need a small-ϵ approximation. Since such bodies increase the stream velocity by only a small amount, λ is small when ϵ is small; in fact it is *at least* as small as ϵ itself. Hence even without further information about the dependence of

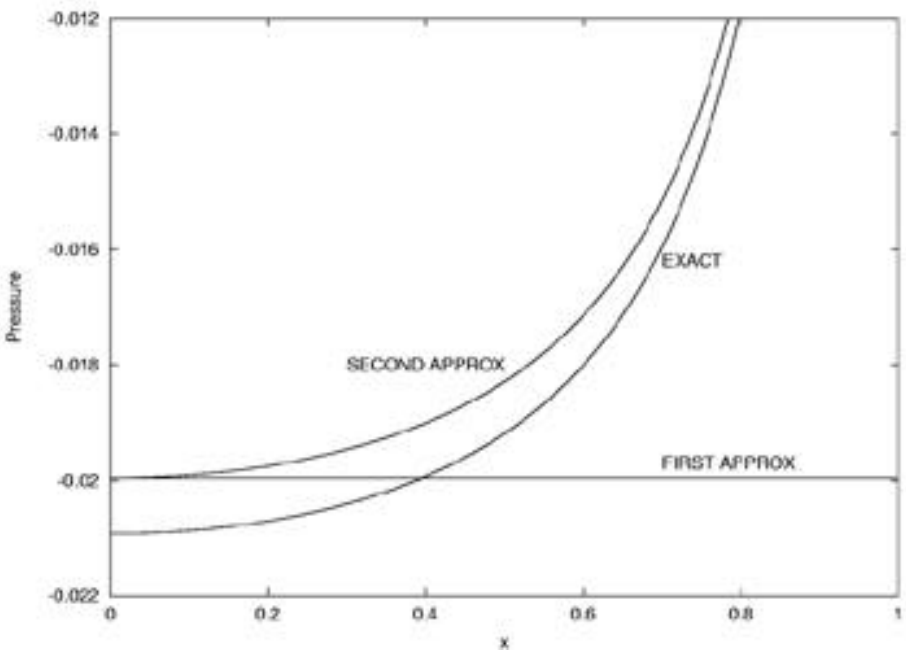

Figure 5: Pressure on spheroid with slenderness $\epsilon = 0.1$.

λ on ϵ, we can approximate the denominator of (24) by 1, to give (in both 2D and 3D)

$$p(x) = -\lambda - \frac{1}{2}\,\lambda^2 + \frac{1}{2}\,\frac{\epsilon^2 x^2}{1-x^2} \tag{27}$$

with error of order at most ϵ^3. But then since λ is small we can also neglect the term in λ^2 relative to that in λ, giving

$$p(x) = -\lambda + \frac{1}{2}\,\frac{\epsilon^2 x^2}{1-x^2}\,, \tag{28}$$

now with errors of order at most the maximum of λ^2 and ϵ^3.

This is most obvious in 2D for ellipses since $\lambda = \epsilon$ exactly, and the error in (28) is of order ϵ^2. But in that case the second term of (28) is also small within the above error range, and can and should be neglected relative to the first term (so long as $|x|$ is not too close to 1), leading to the constant pressure

$$p(x) = -\epsilon \tag{29}$$

on thin ellipses, a result with order ϵ^2 error, as already obtained by the thin-body theory. If we revert to (27), we obtain a more accurate but non-constant result for ellipses, of the form

$$p(x) = -\epsilon - \frac{1}{2}\,\epsilon^2 + \frac{1}{2}\,\frac{\epsilon^2 x^2}{1-x^2}\,, \tag{30}$$

now with formal error of order ϵ^3, but which happens to be exact at $x = 0$. Both approximations are displayed (as the horizontal line "FIRST APPROX" and the curve "SECOND APPROX") relative to the "EXACT" solution, in Figure 4 for $\epsilon = 0.1$.

Again the 3D result for spheroids is somewhat more complicated. Now by small-ϵ expansion of the exact result (26) we find a much smaller relative increase in velocity, namely

$$\lambda = -\epsilon^2 \left[\log\frac{\epsilon}{2} + 1\right] + O(\epsilon^4 \log^2 \epsilon) \tag{31}$$

so (28) becomes

$$p(x) = \epsilon^2 \left[\log\frac{\epsilon}{2} + 1\right] + \frac{1}{2}\,\frac{\epsilon^2 x^2}{1-x^2} \tag{32}$$

which has an error of order $\epsilon^4 \log^2 \epsilon$. Equation (32) is thus a very accurate approximation so long as $|x|$ is not too close to 1, but does *not* predict constant pressure on slender spheroids. It is displayed for $\epsilon = 0.1$ as the "SECOND APPROX" curve of Figure 5, relative to the "EXACT" curve.

The approximation (32) also follows from the general slender body formula (19) noting that for the spheroid $f(x) = \epsilon\sqrt{1-x^2}$, we have $A(x) = B(x) = -\epsilon^2 x$, and the argument of the logarithm in (19) is $\epsilon/2$, so the first two terms of (19) yield the constant part of (32), while the remaining two terms yield the non-constant part. The denominator of (24) is also restored if the end correction factor (20) is applied.

Is the pressure on a slender spheroid in 3D then not constant to a leading order of approximation, as it was on a thin ellipse in 2D? Well, yes in a sense the pressure can be said to be constant, but only as a very crude first approximation. If we drop the second term of (32), we leave a constant pressure

$$p(x) = \epsilon^2 \left[\log\frac{\epsilon}{2} + 1\right] \tag{33}$$

on a slender spheroid, but we have now made an absolute error of order ϵ^2. The constant term (33) that then remains is of order $\epsilon^2 \log \epsilon$, so we have made

a relative error of order $1/\log\epsilon$, and ϵ must be exceedingly small for this to be justified. The approximation (33) at $\epsilon = 0.1$ is shown as the horizontal line labelled "FIRST APPROX" in Figure 5.

The danger of neglecting order ϵ^2 terms relative to order $\epsilon^2 \log\epsilon$ terms is illustrated by the fact that if we do wish to drop the second term of (32), consistently we should also drop the "+1" inside the square bracket of the first term and even the factor " 1/2 " inside the logarithm, since these terms also contribute order ϵ^2 to the final answer. In fact, with the same formal order ϵ^2 error, (33) can be replaced by

$$p(x) = \epsilon^2[\log\epsilon + k] \tag{34}$$

for any finite constant k. It is hardly comfortable to have to deal with an approximation which has such a large element of non-uniqueness.

However, one redeeming feature of the approximation (33), or of (34) with $k = 1 - \log 2 \approx 0.31$, is that it is a good approximation (with much smaller formal error, of order $\epsilon^4 \log^2\epsilon$) to the pressure at the centre station $x = 0$, where the second term of (32) vanishes. Hence the FIRST APPROX and SECOND APPROX agree at $x = 0$ in Figure 5. This enables a quantitative measure of constancy of pressure. In general as x varies, the pressure coefficient rises from its (small negative) value at $x = 0$, and we may ask how small must ϵ be in order that this rise is small relative to the pressure magnitude at $x = 0$.

For example, suppose we fix attention on a point where $x^2 = 1/2$, or $x \approx 0.7$. Then the absolute rise in p between the centre station and this station is $\epsilon^2/2$, both for ellipses and spheroids. However, this is relatively much more significant in the latter case than the former. Thus in order for the pressure magnitude at this point to be at most 10% different from than that at $x = 0$, it is only necessary for ϵ to be smaller than 0.2 for ellipses, but ϵ must be smaller than $2e^{-6} \approx 0.005$ for spheroids. This comparison is even more severe closer to the ends, e.g. if we require such pressure constancy as far from the centre as $x^2 = 2/3$ or $x \approx 0.8$, where the absolute rise is ϵ^2, then we require $\epsilon < 0.1$ for ellipses, but a quite unrealistic $\epsilon < 2e^{-11} \approx 0.000033$ for spheroids.

Slender bodies with near-constant pressure

If the pressure is not constant on a spheroid, is there any body of revolution on which the pressure is constant? The exact answer is certainly no, but we only require a slender-body approximation. Specifically we seek shapes $f(x)$ such that the pressure $p(x)$ given by (19) takes a constant (small negative) value p_0, for all x not close to the ends. This can be done in a straightforward numerical manner by forcing $p(x_n) = p_0$, at a set of N collocation points $x = x_n,\ n = 1, \ldots, N$, which can lie in $0 \le x < 1$ using symmetry. If we specify $f(x)$ by a set of N parameters, this yields a set of N nonlinear algebraic equations in the N unknown parameters, which can be solved by Newton's method.

A convenient parametrisation of the body shape is obtained by the Legendre series

$$A(x) = \sum_{n=1}^{N} a_n P_{2n-1}(x) \tag{35}$$

where $P_N(t)$ is the Legendre polynomial, and a_n are the N coefficients to be determined. Then

$$B(x) = \sum_{n=1}^{N} a_n \sigma_{2n-1} P_{2n-1}(x) \tag{36}$$

where $\sigma_n = 1 + 1/2 + 1/3 + \ldots + 1/n$, and

$$\frac{1}{2} f(x)^2 = \int_1^x A(x)dx = \sum_{n=1}^{N} \frac{a_n}{4n-1} \left[P_{2n}(x) - P_{2n-2}(x) \right] \tag{37}$$

so all quantities required for (19) can be computed readily, given the coefficients a_n. The spheroid is the particular case $N = 1$, with $a_1 = -\epsilon^2$.

The numerical results for large N depend to a certain extent on the choice of the collocation points x_n, and ultimate refinement of this choice and of the present numerical method was not sought. A satisfactory grid was $x_n = (n-1)/(N+1)$, for which convergence (e.g. of $f(0) = \epsilon$ as N increases) to about 4 figures was achieved by $N = 22$. The coefficients a_n decrease in size quite rapidly, with for example a_{20} generally of the order of 10^{-8}, compared to a_1 of the order of 10^{-2}. The final pressure is constant to more than 4 figures not only at the grid points, but also for all x less than x_{N-1}, then constant to 3 figures (falling slightly) between x_{N-1} and x_N, before increasing rapidly for $x > x_N$, i.e. for $x > 0.91$ at $N = 22$, but at $N = 22$ remaining within 10% of p_0 up to $x = 0.93$.

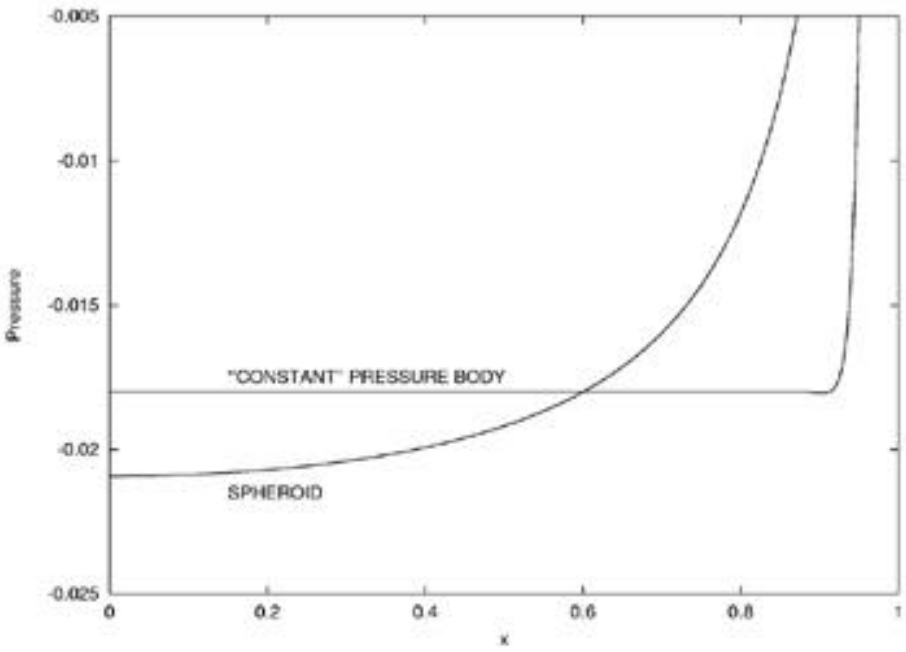

Figure 6: Pressure on "constant"-pressure body with slenderness $\epsilon = 0.1$, compared to exact pressure on spheroid with the same slenderness.

It is clearly impossible to maintain constancy of pressure right to the ends. This is true whether or not the uniformising factor (20) is used; with it, the extreme end pressure is finite, without it infinite, but in neither case is the end pressure small and negative. In practice, it made very little difference to the numerical results whether (20) was or was not used, and loss of pressure constancy in about the last 7% of the length seems inevitable. Further work is needed to assess whether this breakdown range can be reduced. In any case, the present extent of constancy of pressure far exceeds that for a spheroid, as indicated by the comparison in Figure 6 for $\epsilon = 0.1$.

Figure 7 shows the final body shape $r = f(x)$ at $p_0 = -0.018$, which generates a body with width/length ratio $\epsilon = 0.10$, compared to a spheroid of the same slenderness. As we increase $|p_0|$, the body becomes less slender, and eventually the procedure fails. This is signalled first by a loss of convexity at about $p_0 = -0.030$ or $\epsilon = 0.14$, with $f'(0) > 0$. All "constant" pressure bodies less slender than this are dumbell-shaped.

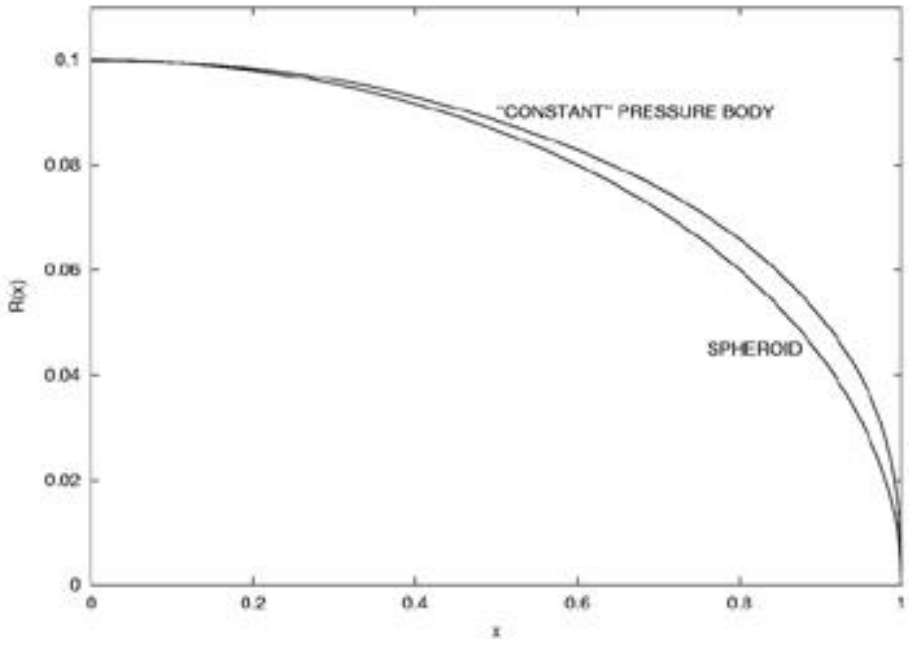

Figure 7: Shape of "constant"-pressure body compared to spheroid.

Within the whole range of convex bodies, the computed relation between slenderness ϵ and pressure $p = p_0$ is quite accurately represented by (34) with $k = 0.50$, which is to be compared to $k = 0.31$ for the spheroid result (33).

Relationship to long cavities

Although in principle the present work is independent of the particular application to supercavitation, this area is one where there has been a significant amount of experimental, empirical and computational effort, see e.g Tulin (1998), and several review articles in Michel (2001). In this application, the closed "body" of interest is a combination of a relatively short rigid "cavitator" or nose, which has a prescribed shape and on which the pressure is not necessarily constant, a much longer attached cavity, on which the pressure is required to be constant, and another short region of cavity collapse at the trailing end. In supercavitation the constant negative non-dimensional pressure is written as $p_0 = -\sigma/2$, where σ is the "cavitation number".

Hence the present theory is relevant to the slender-body limit in which the cavity length far exceeds the cavitator length, and the cavitation number is small. In a sense this is no different from the numerical consequences in the previous section of seeking approximate solutions for "constant" pressure bodies, where we must allow the pressure to be non-constant near the ends of the body. Those end regions can then act as surrogates for the cavitator and collapse region, and indeed an early study of supercavitation by Reichardt (1946) already used this approach.

Significant interest in supercavitation lies in relationships between cavitator geometry and cavity dimensions. There are empirical formulae indicating that the length and width of the cavity (relative to the length of the cavitator) are each proportional to the square root of a drag coefficient which characterises the geometry of the cavitator. Hence the slenderness ϵ or width/length ratio of the cavitator-cavity combination is (at least according to these formulae) independent of the drag coefficient, and thus independent of the shape of the cavitator, depending only on the cavitation number σ.

For two-dimensional supercavitation, the thin-body theory of Tulin (1953) indicates that $\sigma = 2\epsilon$, and that the cavity is asymptotically elliptical. This agrees with the conclusion that to leading order in ϵ, the pressure on a thin ellipse is constant and of magnitude $p_0 = -\epsilon$, with a consistently small $O(\epsilon^2)$ error.

The equivalent result for axisymmetric three-dimensional supercavitation is a little more problematic. If we are prepared to neglect terms with relative error $O(1/\log\epsilon)$, then the cavity is asymptotically spheroidal and (34) implies that

$$\sigma = -2\epsilon^2(\log\epsilon + k) \tag{38}$$

for some constant k. This constant k is formally arbitrary, although if the cavity were exactly spheroidal, $k = 0.31$ might be preferred. However, the cavity is only spheroidal to a very crude approximation, and if we abandon the spheroidal assumption, then there is no formal asymptotic justification for (38) at any k. On the other hand, if the cavity asymptotes to one of the "constant"-pressure bodies constructed in the previous section, then since we have found that these bodies have a pressure close to (34) with $k = 0.50$, a case can be made for use of (38) with $k \approx 0.5$.

Figure 8 shows graphs of σ versus ϵ from (38) for $k = 0.3, 0.5, 0.7$, compared to supercavitation results of May (1975), Savchenko (in Michel 2001) and Garabedian (1956). The May and Savchenko curves are empirical fits

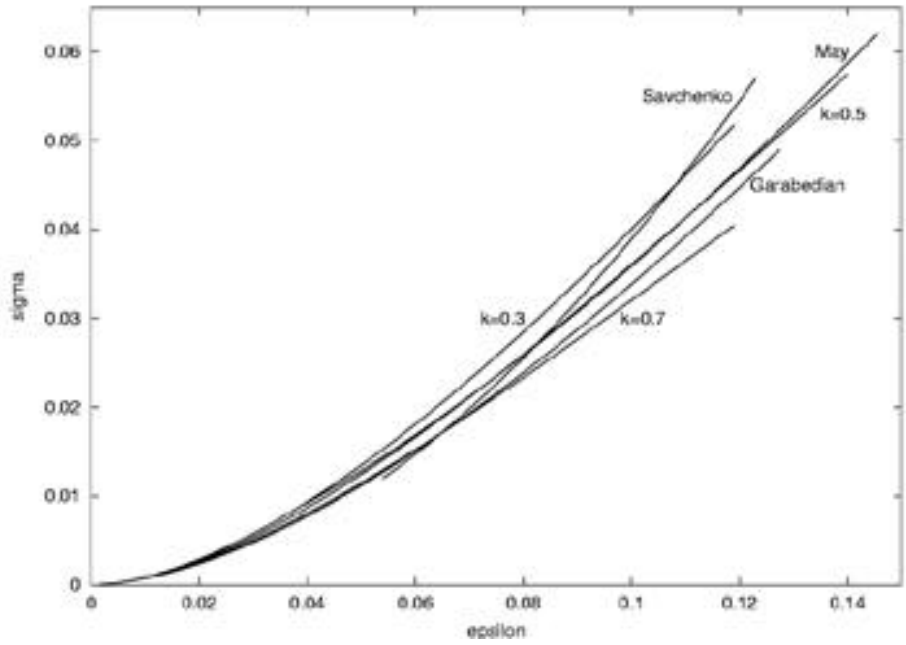

Figure 8: Cavitation number σ versus slenderness ϵ from (38) with $k = 0.3, 0.5, 0.7$, compared to supercavitation results of May, Savchenko and Garabedian.

to experimental measurements. The May curve is very close to the present $k = 0.5$ curve. The Savchenko curve is close to $k = 0.7$ at the more slender end of the experimental range, and to $k = 0.3$ at the less slender end, with $k = 0.5$ being a reasonable compromise value. The Garabedian curve is a theoretical formula based on neglect of terms with relative error $O(1/\log\sigma)$, which is almost (but not quite!) the same thing as neglect of terms with relative error $O(1/\log\epsilon)$, and seems to give results between $k = 0.6$ and $k = 0.7$, which are also very close to an empirical formula of Reichardt (1946). Other experimental, empirical or computational results are quoted in articles in Michel (2001), which also fall in about the range $0.3 < k < 0.7$ of Figure 8.

Other applications of slender-body theory

General inner limit and drag

Let us turn to more general slender-body theories. There are a number of such theories which use a distribution of 3D or point sources along the x-axis, with a varying strength $m(x)$ which often can be shown to be equal to $US'(x)$ where U is the free stream velocity (normalised here to 1) and $S(x)$ is the body section area. If the potential of a unit 3D source at the origin is written $G_3(x, y, z)$, we need the limit of such a line distribution as $r = \sqrt{y^2 + z^2} \to 0$, and expect this to be of the form

$$\int m(\xi) G_3(x - \xi, y, z) d\xi \quad \to \quad m(x)\ G_2(y, z) + b(x) \tag{39}$$

where

$$b(x) = \int m'(\xi) F(x - \xi) d\xi \tag{40}$$

Here $G_2(y, z)$ is the corresponding unit 2D or line source potential in the (y, z) cross-section plane, and $F(x)$ is a suitable kernel function. At each fixed station x, the first term on the right of (39) is "local", depending only on the current value of $m(x)$. If the source strength $m(x)$ is not constant, there is an additional "non-local" term $b(x)$, whose value at station x in principle depends on values of the axial rate of change of source strength $m'(\xi)$ at all other stations ξ, expressed as a convolution integral (40) with weighting function $F(x - \xi)$.

For the simple prototype problem considered so far, namely irrotational flow of an incompressible inviscid fluid past a single fixed impermeable body, we have

$$G_3(x, y, z) = -\frac{1}{4\pi} \frac{1}{\sqrt{x^2 + r^2}} \tag{41}$$

$$G_2(y, z) = \frac{1}{2\pi} \log(r) \tag{42}$$

and

$$F(x) = -\frac{1}{4\pi} \mathrm{sgn}(x) \log 2|x| \tag{43}$$

Here the non-local term captures the essential elliptic character of the prototype boundary-value problem; what we do at one point of space affects what happens everywhere else.

Generalisations of the prototype problem sometimes involve asymptotic results similar to (39) with different 3D source potentials G_3 on the left, but the same or similar functions G_2 and F on the right. In particular there are a number of slender-body problems in which the 2D source G_2 is still given by (42) even though G_3 and F are different. Physically, this can be interpreted as saying that although the 3D problem differs from the prototype, that difference disappears in the 2D near field in the cross-section plane. However, axial changes in the parameters of that (incompressible) 2D flow induce axial velocities via $b(x)$ which are non-local and capture the unique three-dimensionality of the problem.

Various important output quantities follow from the above formalism. For example, local terms (both that already in (39) and others arising from its use to generate the pressure) do not contribute to the drag on the body, which is then due to a contribution $-b'(x)$ to the pressure depending on x alone. Hence the drag is $D = \int S'(x)(-b'(x)dx$ where $S(x)$ is the cross-section area, so after integration by parts,

$$D = \int dx\ S''(x) \int d\xi\ S''(\xi)\ F(x-\xi) \tag{44}$$

Hence for example, d'Alembert's paradox $D = 0$ is verified for the prototype problem, and indeed for any generalisation where $F(x)$ remains an odd function of x as in (43). Otherwise, in evaluating the drag by (44) we can replace $F(x)$ by its even part.

Compressibility

Inclusion of compressibility of the fluid provides a direct generalisation of the prototype problem. Then at free stream Mach number M, the 3D source function is simply obtained by replacing r^2 with $(1-M^2)r^2$ in that (41) for the prototype (incompressible) problem. For subsonic flow with $M < 1$ this can always be done, and the net effect is essentially as if $F(x)$ was still given by (43). The boundary-value problem remains elliptic, and d'Alembert's paradox $D = 0$ still holds.

For supersonic flow with $M > 1$, the 3D source potential must vanish outside of the Mach cone $r = x/\beta$ where $\beta = \sqrt{M^2-1}$, so the range of integration is truncated to $\xi < x - \beta r$. Then we find as we let $r \to 0$ that the local term is again given by the incompressible 2D line source (42), while

the non-local term has kernel

$$F(x) = -\frac{1}{2\pi} \log \frac{2}{\beta} x \tag{45}$$

if $x > 0$, zero otherwise. Now although $b(x)$ still describes non-local effects, it only carries a downstream influence, the contribution at station x only depending on $m(\xi)$ for $\xi \leq x$, thus capturing the essential hyperbolic nature of the original 3D boundary-value problem. Now $F(x)$ is no longer an odd function, and the drag is

$$D = -\frac{1}{4\pi} \int dx \; S''(x) \int d\xi \; S''(\xi) \; \log|x - \xi| \tag{46}$$

This supersonic result was obtained by von Karman and Moore (1932), and improved upon by Lighthill (1945); in fact the supersonic slender body theory was obtained before corresponding incompressible or subsonic slender body theories were derived (see Ward 1955).

Slender ships

Another qualitatively straightforward generalisation is to slender ships moving over a free surface where the linearised disturbance potential must satisfy on the plane $z = 0$ the Kelvin boundary condition

$$g\phi_z + \phi_{xx} = 0 \tag{47}$$

where g is gravity. Then the unit point source potential G_3 satisfying (47) is given by a very complicated formula (Wehausen and Laitone 1960, p.xxx), involving a double integral with respect to the wave number and direction of the water waves. However, again the local term in (39) is just given by the simple line source (42). This now reflects the fact that the near-field limit of the Kelvin condition is $\phi_z = 0$, so the plane $z = 0$ is a plane of symmetry, not supporting waves. This has an immediate local consequence, in that the apparent source strength is related to the section area of the double body, the ship section being reflected in $z = 0$. Thus if $S(x)$ now denotes the true submerged ship section area, $m(x) = 2S'(x)$.

However, the wave-like nature of the original 3D flow is retained in the near field by the non-local term $b(x)$, which now has the kernel function

$$F(x) = -\frac{1}{4\pi} \mathrm{sgn}(x) \log 2|x| - \frac{1}{8} \left[\mathbf{H_0}(gx) + (2 + \mathrm{sgn}(x)) Y_0(g|x|) \right] \tag{48}$$

where $\mathbf{H_0}$ is a Struve function and Y_0 a Bessel function. The first term of (48) is given by (43) as in the prototype problem, and the remaining terms are wave-like. If we formally let $g \to \infty$, these wave-like terms disappear, and in that limit the Kelvin condition becomes (everywhere) the symmetry condition $\phi_z = 0$, so the problem has reduced to the prototype problem for the double body.

Since $\mathbf{H_0}$ is odd, the even part of the kernel $F(x)$ is $-\frac{1}{4}Y_0(g|x|)$, and the drag (44) is

$$D = -\frac{1}{2}\int dx\ S''(x) \int d\xi\ S''(\xi)\ Y_0(g|x-\xi|) \tag{49}$$

which is the slender ship wave resistance formula obtained independently by Vossers (1962), Maruo (1962) and Tuck (1963).

In fact Maruo obtained (49) simply by approximating Michell's (1898) thin-ship wave-resistance integral for small draft. That is, in ship hydrodynamics, to a leading order of approximation, slender-body theory is subsumed in thin-body theory. It is interesting that Michell's integral demands information about the complete offsets $y = \pm Y(x,z)$ of the ship, whereas the slender-ship formula (49) demands only a knowledge of the ship's section area $S(x) = 2\int Y(x,z)dz$. If a computer program for Michell's integral is available, there is no need for a separate computer program for the slender-ship integral (49), since one can simply run the thin-ship code for artificial rectangular sections with offsets $Y(x,z) = S(x)/(2D)$ and an arbitrary small draft D.

However, this subsumption does not apply at higher orders of approximation. Thus as with the prototype problem, the leading order slender-ship potential is second order in the slenderness or beam/length ratio ϵ. In the prototype problem, the next correction to the inner-region potential is of fourth order in ϵ. However, in the presence of a free surface this is no longer the case, and the next term is larger, of third order in ϵ. Not only that, but it depends on nonlinear free-surface terms neglected in the Kelvin boundary condition (47). Hence this correction cannot be subsumed in (linear) thin-ship theory. The effect on the drag is that the slender ship formula (49) gives a 4th-order result, which is subject to a nonlinear 5th-order correction. It would be of considerable interest to compute this correction to the wave resistance, but this does not seem to have been done.

Stokes flows past slender bodies

We now turn to applications of slender body theory where the source strength $m(x)$ is no longer given by the axial rate of change of body section area. One such application is to very viscous flow, described by the Stokes (4th order partial differential) equations. Then internal (irrotational) sources alone are not sufficient to represent the flow about a fixed body, and we also need point singularities generating rotational flow, and contributing to drag forces. For slender bodies of revolution $r = f(x)$, the appropriate generators are then axial distributions of both point sources and point "Stokeslets".

It turns out that in this problem, the source distribution plays a minor role, not contributing to the leading-order slender-body approximation. If the Stokeslet strength is now written $m(x)$, satisfaction of the no-slip boundary condition on $r = f(x)$ demands that

$$\frac{m(x)}{2\pi}\left[\log f(x) + \frac{1}{2}\right] + b(x) = -\frac{1}{2} \tag{50}$$

or on $(-1, 1)$ that $m(x)$ satisfy the integral equation

$$\frac{m(x)}{2\pi}\left[\log \frac{f(x)}{2\sqrt{1-x^2}} + \frac{1}{2}\right] + \frac{1}{4\pi}\int_{-1}^{1} \frac{m(x) - m(\xi)}{|x-\xi|}\, d\xi = -\frac{1}{2} \tag{51}$$

Although the Legendre series (27) provides a convenient way to discretise (51) for numerical purposes, there are a number of serious difficulties, especially at the ends, of a character similar to that encountered earlier when attempting to force the pressure in the prototype problem to be everywhere constant. A simple alternative (Tuck 1968) is to use inverse methods, in which $m(x)$ is given, and the shape $f(x)$ is determined by (51).

Solid mechanics for elongated loads

A somewhat similar application in solid mechanics (Kalker 1972, Tuck and Mei 1983) is to a "slender punch", i.e. a load applied to a finite elongated region of the plane free boundary of an elastic half-space. This has applications to elongated footings for buildings. The similarity to Stokes flow arises from the 4th-order nature of the partial differential equations describing the problem.

Suppose the punch lies in $|y| < f(x)$, and let $m(x)$ be the (downward) force per unit length that it exerts. Then the downward displacement $w(x)$

under the punch can be shown to be proportional to the potential ϕ of a line of sources $m(x)$ as in the prototype problem, i.e. as given in the near field by (13), evaluated for frictionless punches at $r = f(x)/2$. Specifically

$$\frac{1}{2}\frac{\mu}{1-\nu}w(x) = \frac{m(x)}{2\pi}\log\left[\frac{1}{2}f(x)\right] + b(x) \tag{52}$$

where μ and ν are the elastic (Lame) constants. If there is adhesion, the point of evaluation differs from $r = f(x)/2$, but one can then define an "effective frictionless width" (Tuck and Mei 1983) replacing and increasing the actual punch width $2f(x)$.

If the load $m(x)$ is given, on a given punch width $2f(x)$, equation (52) with $b(x)$ determined from $m(x)$ by (14) or (15) gives the resulting displacement $w(x)$ directly. However, again it is a much more difficult task to solve for the load $m(x)$, given the displacement $w(x)$, since we then have to solve the integral equation

$$\frac{1}{2}\frac{\mu}{1-\nu}w(x) = \frac{m(x)}{2\pi}\log\left[\frac{f(x)}{4\sqrt{1-x^2}}\right] + \frac{1}{4\pi}\int_{-1}^{1}\frac{m(x)-m(\xi)}{|x-\xi|}\,d\xi \tag{53}$$

for $m(x)$. Equation (53) is quite similar to that (51) for slender-body Stokes flow, and leads to similar difficulties at the ends (Panek and Kalker 1977, Tuck and Mei 1983).

Slender moonpools

Let me mention a final application of slender-body ideas, even more remote from the original prototype problem, in that it does not involve a streaming flow, or indeed even a "body". The application is to sloshing of water waves in an elongated basin. If this basin is fully enclosed, as in a swimming pool or lake, there are interesting asymptotic issues for slender basins, concerned with the seiching modes of motion along the basin, but these issues have little in common with the source-distribution models discussed in the present paper. In particular, if the water level at one station x falls, it must rise instantly at other stations to conserve mass, and the flow in the bounded cross-section at station x cannot have a source-like character.

However, suppose the "basin" is not closed, having access at each station x to an ocean of infinite depth. Then when the water level at that station falls, the outward volume flux so generated can pass to infinity in a source-like manner. The water level then need not immediately rise at other stations.

For example, the basin may be a "moonpool" (Molin 2001), a hole giving access to water beneath an otherwise rigid boundary. This boundary could be the bottom of the hull of a drilling ship, or perhaps an ice sheet. Here we idealise the boundary to be a rigid sheet of infinite extent and zero thickness, and the water to be of infinite extent and depth, and let the moonpool be elongated in the x-direction.

Now if sloshing is taking place in this moonpool, with a water level varying with x, there will be an apparent source at each station x, of some strength $m(x)$ to be determined, and hence if the moonpool is slender, the flow will appear in the far field to be generated by a line distribution of point sources of strength $m(x)$ as in (2). Note that there are no waves in the far field – of course there cannot be waves there, since the "free" surface there is rigid!

On the other hand, if we move into the near field, with r reduced to the size of the width of the moonpool, we shall see water waves, with a rise or fall of the water level in the moonpool. Hence we need again the inner limit (39). Details of the 2D wave-like inner flow will be omitted here (see Tuck and Newman 2002).

However, what is clear without such detail is that, for moonpools with a rectangular planform, there is a necessity for the *whole* disturbance potential ϕ in the near field as given by (39) to have the identical x-variation along the pool. That is, the non-local term $b(x)$ needs to be proportional to the local source strength $m(x)$. If the proportionality constant is μ, we therefore have to solve an eigenvalue problem, for the integro-differential equation

$$\int m'(\xi)F(x-\xi)d\xi = \mu m(x) \tag{54}$$

with $F(x)$ given by (43). For a pool in $(-1,1)$, the truncated Legendre series (35) is a convenient tool for numerical solution of this problem, and the first three eigenvalues in increasing order are given by

$$2\pi\mu + \log 2 = 0.2332, 1.4437, 1.9409, \ldots \tag{55}$$

The first three eigenmodes $m(x)$ are shown in Figure 9. The lowest-order mode is a symmetric "pumping" mode which does not have an equivalent for a closed pool, as there is a non-zero net volume of water-surface displacement, which would not conserve mass if the pool was closed. The second (antisymmetric) mode has a nodal point at the centre station $x = 0$ and is the fundamental longitudinal "sloshing" mode. The third mode is symmetric with two nodal points, and is also of a pumping nature. All of these

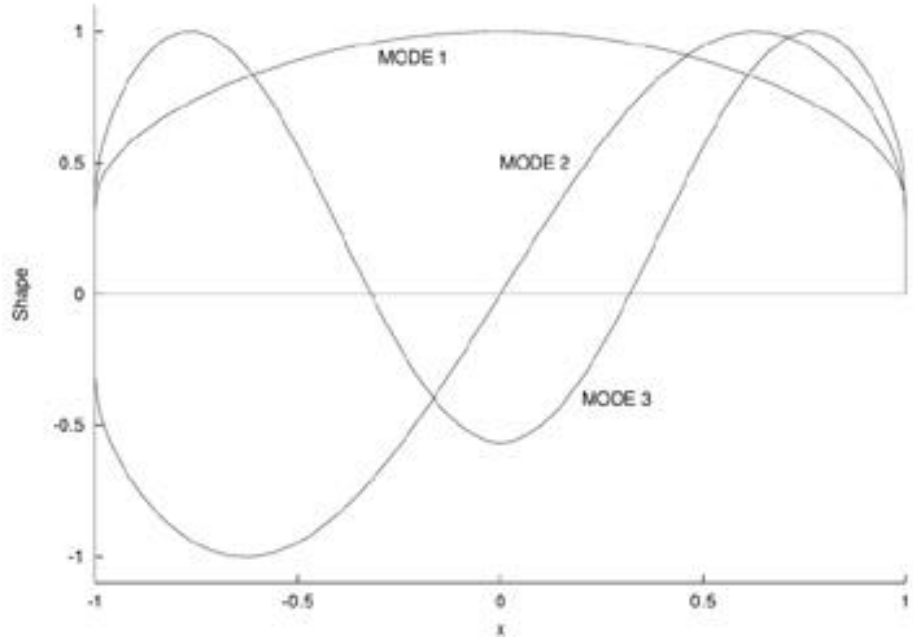

Figure 9: The first three longitudinal moonpool modes.

modes seem numerically to have infinite slope at the ends $|x| = 1$, though this matter has not yet been investigated analytically.

Conclusions

(to be written)

Acknowledgements

(to be written)

References

(to be completed)

Ashley and Landahl 1966

Garabedian, P.R., "Calculation of axially symmetric cavities and jets", *Pacific J. Math.* **6** (1956) 611–689.

Haese P.M., " ", PhD thesis, The University of Adelaide, 2002.

Kalker, J.J., "On elastic line contact", *J. Appl. Mech. ASME* **39** (1972) 1125–1132.

Karman, T. von and Moore, N.B., "Resistance of slender bodies moving with supersonic velocities", *Trans. ASME* **54** (1932) 303–310.

Lamb, H., "Hydrodynamics", Cambridge University Press, 6th edn., 1932.

Lighthill, M.J., "Supersonic flow past bodies of revolution", *Rep. Mem. Aero. Res. Council*, no. 2003, London 1945.

Lighthill 1949

Lighthill, M.J. "A new approach to thin aerofoil theory", *Aero. Quart.* **3** (1951) 193–210.

Maruo, H., "Calculation of the wave resistance of ships the draught of which is as small as the beam", *J. Zosen Kiokai Japan* **112** (1962) 161.

May, A., "Water entry and the cavity-running behavior of missiles", SEAHAC Technical Report 75-2, *Naval Surface Weapons Center*, Silver Spring, Maryland, 1975.

Michel, J.-M., (ed.) *Supercavitating Flows*, von Karman Institute for Fluid Dynamics, Brussels, February 2001.

Michell, J. H., "The wave resistance of a ship", *Phil. Mag.* **45** (1898) 106–123.

Molin, B., "On the piston and sloshing modes in moonpools", *J. Fluid Mech.* **430** (2001) 27–50.

Panek, C. and Kalker, J.J., "A solution for the narrow rectangular punch", *J. Elasticity* **7** (1977) 213–218.

Reichardt, H., "The laws of cavitation bubbles at axially symmetrical bodies in a flow", *Min. Aircraft Prod. Volkenrode*, Reports and Translations **766**, ONR, 1946.

Tuck, E.O., "The steady motion of a slender ship", PhD thesis, Cambridge University, 1963.

Tuck, E.O., "Some methods for flows past blunt slender bodies", *J. Fluid Mech.* **18** (1964) 619–635.

Tuck, E.O., "Toward the calculation and minimization of Stokes drag on bodies of arbitrary shape", *3rd Australasian Conference on Hydraulics and Fluid Mech.*, Sydney, Inst. Engrs. Aust. (1968) pp. 29–32.

Tuck, E.O., "Analytic aspects of slender body theory", in Wave Asymptotics, ed. Martin P.A. and Wickham, G.R., Cambridge University Press, 1992, pp. 184–201.

Tuck, E.O. and Mei, C.C., "Contact of one or more slender bodies with an elastic half space", *Int. J. Solids Structures* **19** (1983) 1–23.

Tuck, E.O. and Newman, J.N., "Longitudinal waves in slender moonpools", 17th Int. Workshop on Water Waves and Floating Bodies, Cambridge, April 2002. Proc. ed. R. Rainey, Roy. Inst. Naval Archs., London.

Tuck, E.O. and Scullen, D.C., "A comparison of linear and nonlinear computations of waves made by slender submerged bodies", *J. Engg. Math.* **42** (2002) 255–264.

Tuck, E.O., Scullen, D.C. and Lazauskas, L., "Wave patterns and minimum wave resistance for high-speed vessels", 24th Symposium on Naval Hydrodynamics, Fukuoka, Japan, July 2002. Proc. Office of Naval Research, Washington D.C.

Tulin, M.P., "Steady two-dimensional cavity flows about slender bodies", *David Taylor Model Basin*, Rep. 834, Department of the Navy, 1953.

Tulin, M.P., "On the shape and dimensions of three-dimensional cavities in supercavitating flows", *Applied Scientific Research* **58** (1998) 51–61.

Vossers, G., "Some applications of the slender body theory in ship hydrodynamics", PhD thesis, Delft University, 1962.

Ward, G.N., "Linearised theory of steady high-speed flow", Cambridge University Press, 1955.

Wehausen, J.V. and Laitone E.V., "Surface Waves", in *Handb. Phys.* **9**, Springer-Verlag, 1960.